PHYSICAL REVIEW D **71,** 095007 (2005)

Update on the direct detection of supersymmetric dark matter

John Ellis,[1] Keith A. Olive,[2] Yudi Santoso,[3] and Vassilis C. Spanos[2]
[1]*TH Division, CERN, Geneva, Switzerland*
[2]*William I. Fine Theoretical Physics Institute, University of Minnesota, Minneapolis, Minnesota 55455, USA*
[3]*Department of Physics, University of Guelph, Guelph, Ontario N1G 2W1, Canada*
and Perimeter Institute of Theoretical Physics, Waterloo, Ontario N2L 2Y5, Canada
(Received 9 February 2005; published 12 May 2005)

We compare updated predictions for the elastic scattering of supersymmetric neutralino dark matter with the improved experimental upper limit recently published by Cryogenic Dark Matter Search (CDMS) II. We take into account the possibility that the π-nucleon Σ term may be somewhat larger than was previously considered plausible, as may be supported by the masses of exotic baryons reported recently. We also incorporate the new central value of m_t, which affects indirectly constraints on the supersymmetric parameter space, for example, via calculations of the relic density. Even if a large value of Σ is assumed, the CDMS II data currently exclude only small parts of the parameter space in the constrained minimal standard model (CMSSM) with universal soft supersymmetry-breaking Higgs, squark, and slepton masses. None of the previously proposed CMSSM benchmark scenarios is excluded for any value of Σ, and the CDMS II data do not impinge on the domains of the CMSSM parameter space favored at the 90% confidence level in a recent likelihood analysis. However, some models with nonuniversal Higgs, squark, and slepton masses and neutralino masses $\lesssim 700$ GeV are excluded by the CDMS II data.

DOI: 10.1103/PhysRevD.71.095007 PACS numbers: 12.60.Jv, 95.35.+d

I. INTRODUCTION

The lightest supersymmetric particle (LSP) is stable in models in which R parity is conserved, in which case it is a suitable candidate for the cold dark matter required by astrophysical and cosmological observations [1]. One of the generic possibilities is that the LSP is the lightest neutralino χ, in which case the detection of dark matter appears feasible. The direct detection of supersymmetric dark matter via scattering on nuclei in deep-underground, low-background experiments has been discussed many times [2–9].

There are, however, three reasons why a reevaluation of the prospects for such experiments is now timely. The first is the motivation provided by the upper limit on the dark-matter scattering cross section provided by the CDMS II experiment [10], which is substantially more stringent than previous experiments [11]. The CDMS II result appears, in particular, to conflict with the dark-matter scattering interpretation of the results of the previous Dark Matter searches at Gran Sasso laboratory (DAMA) experiment [12]. A second reason is evolution in standard model inputs into the calculation of the scattering matrix elements. Recent particle-physics experiments tend to favor a value of the pion-nucleon sigma term Σ that is somewhat higher than earlier experiments, favoring a larger theoretical estimate for the spin-independent part of the dark-matter scattering cross section [13]. Interestingly, a larger value of Σ also is favored independently by hints from the spectroscopy of pentaquark baryons, if they exist [14]. We also include the effect of the new preferred value of m_t [15] on the supersymmetric parameter space and on relic-density calculations. Finally, there has been some progress recently in understanding which parts of parameter space are favored in certain versions of the minimal supersymmetric extension of the standard model (MSSM). In particular, if the input soft supersymmetry-breaking parameters are constrained to be universal (CMSSM), the data on m_W, $\sin^2\theta_W$ and $g_\mu - 2$ all favor independently a relatively low mass for the lightest neutralino [16], favoring in turn a relatively large dark-matter scattering cross section.

It is the purpose of this paper, in light of these developments, to reevaluate the prospects for discovering dark-matter scattering in forthcoming experiments. We include in our analysis not only models in which neutralinos are the dominant source of cold dark matter, but also those in which neutralinos provide only some fraction $f_\chi < 1$. In the latter case, we assume that neutralinos constitute the same fraction $f_\chi < 1$ of the galactic halo. For comparison with experiments searching for dark-matter scattering, which usually assume that all the halos are composed of neutralinos, we rescale the effective scattering cross section by the same factor $f_\chi < 1$.

We find that, even with the larger value of Σ, only very small parts of the CMSSM parameter space are excluded by the current CDMS II result. Specifically, none of the benchmark scenarios proposed recently [17] is excluded, and neither is any of the 90% confidence level region favored in a recent likelihood analysis of the CMSSM [16]. On the other hand, if one relaxes universality for the squark, slepton, and Higgs masses, so as to consider the most general low-energy effective supersymmetric theory (LEEST), some models with $m_\chi \lesssim 700$ GeV are excluded for large Σ. We reach a similar conclusion even if the squark and slepton masses are assumed to be equal, and we allow only nonuniversal Higgs masses (NUHM).

Indeed, as we discuss, the dominant mechanism leading to a large cross section is the reduction in the magnitude of the Higgs superpotential mixing parameter μ and the pseudoscalar Higgs mass m_A allowed by the relaxed electroweak vacuum conditions in the NUHM.

II. SPIN-INDEPENDENT χ-NUCLEON SCATTERING MATRIX ELEMENTS

A. Model-dependent supersymmetric operator coefficients

We assume that the neutralino LSP χ is the lightest eigenstate of the mixed Bino $\tilde{B}$, Wino $\tilde{W}$, and Higgsino $\tilde{H}_{1,2}$ system, whose mass matrix N is diagonalized by a matrix Z: $\mathrm{diag}(m_{\chi_{1,\ldots,4}}) = Z^* N Z^{-1}$, with

$$\chi = Z_{\chi 1}\tilde{B} + Z_{\chi 2}\tilde{W} + Z_{\chi 3}\tilde{H}_1 + Z_{\chi 4}\tilde{H}_2. \tag{1}$$

We neglect the possibility of CP violation and assume universality at the supersymmetric grand unified theory (GUT) scale for the U(1) and SU(2) gaugino masses: $M_{1,2} = m_{1/2}$, so that $M_1 = \frac{5}{3}\tan^2\theta_W M_2$ at the electroweak scale.

The following low-energy effective four-fermion Lagrangian describes spin-independent elastic χ-nucleon scattering:

$$\mathcal{L} = \alpha_{3i}\bar{\chi}\chi\bar{q}_i q_i, \tag{2}$$

which is to be summed over the quark flavors q and the subscript i labels up-type quarks ($i = 1$) and down-type quarks ($i = 2$). The model-dependent coefficients α_{3i} are given by

$$\begin{aligned}\alpha_{3i} = &-\frac{1}{2(m_{1i}^2 - m_\chi^2)}\,\mathrm{Re}[(X_i)(Y_i)^*] \\ &-\frac{1}{2(m_{2i}^2 - m_\chi^2)}\,\mathrm{Re}[(W_i)(V_i)^*] \\ &-\frac{g m_{qi}}{4 m_W B_i}\Bigg[\mathrm{Re}(\delta_{1i}[gZ_{\chi 2} - g'Z_{\chi 1}]) \\ &\times D_i C_i\left(-\frac{1}{m_{H_1}^2} + \frac{1}{m_{H_2}^2}\right) + \mathrm{Re}(\delta_{2i}[gZ_{\chi 2} - g'Z_{\chi 1}]) \\ &\times\left(\frac{D_i^2}{m_{H_2}^2} + \frac{C_i^2}{m_{H_1}^2}\right)\Bigg],\end{aligned} \tag{3}$$

where

$$\begin{aligned}X_i &\equiv \eta_{11}^*\frac{g m_{q_i} Z_{\chi 5-i}^*}{2 m_W B_i} - \eta_{12}^* e_i g' Z_{\chi 1}^*, \\ Y_i &\equiv \eta_{11}^*\left(\frac{y_i}{2}g' Z_{\chi 1} + g T_{3i} Z_{\chi 2}\right) + \eta_{12}^*\frac{g m_{q_i} Z_{\chi 5-i}}{2 m_W B_i}, \\ W_i &\equiv \eta_{21}^*\frac{g m_{q_i} Z_{\chi 5-i}^*}{2 m_W B_i} - \eta_{22}^* e_i g' Z_{\chi 1}^*, \\ V_i &\equiv \eta_{22}^*\frac{g m_{q_i} Z_{\chi 5-i}}{2 m_W B_i} + \eta_{21}^*\left(\frac{y_i}{2}g' Z_{\chi 1} + g T_{3i} Z_{\chi 2}\right),\end{aligned} \tag{4}$$

with y_i, T_{3i} denoting hypercharge and isospin, and

$$\delta_{1i} = Z_{\chi 3}(Z_{\chi 4}), \qquad \delta_{2i} = Z_{\chi 4}, (-Z_{\chi 3}), \tag{5}$$

$$\begin{aligned}B_i = \sin\beta(\cos\beta), \qquad C_i = \sin\alpha(\cos\alpha), \\ D_i = \cos\alpha(-\sin\alpha),\end{aligned} \tag{6}$$

for up (down) type quarks. We denote by $m_{H_2} < m_{H_1}$ the two scalar Higgs masses, and α denotes the Higgs mixing angle. Finally, we note that the factors η_{ij} arise from the diagonalization of the squark mass matrices: $\mathrm{diag}(m_1^2, m_2^2) \equiv \eta M^2 \eta^{-1}$, which can be parameterized for each flavor f by an angle θ_f and phase γ_f:

$$\begin{pmatrix} \cos\theta_f & \sin\theta_f e^{i\gamma_f} \\ -\sin\theta_f e^{-i\gamma_f} & \cos\theta_f \end{pmatrix} \equiv \begin{pmatrix} \eta_{11} & \eta_{12} \\ \eta_{21} & \eta_{22} \end{pmatrix}. \tag{7}$$

In the models we study below, the squark flavors are diagonalized in the same basis as the quarks.

B. Hadronic matrix elements

The scalar part of the cross section can be written as

$$\sigma_3 = \frac{4 m_r^2}{\pi}[Z f_p + (A - Z) f_n]^2, \tag{8}$$

where m_r is the reduced LSP mass,

$$\frac{f_p}{m_p} = \sum_{q=u,d,s} f_{Tq}^{(p)}\frac{\alpha_{3q}}{m_q} + \frac{2}{27} f_{TG}^{(p)}\sum_{c,b,t}\frac{\alpha_{3q}}{m_q}, \tag{9}$$

the parameters $f_{Tq}^{(p)}$ are defined by

$$m_p f_{Tq}^{(p)} \equiv \langle p|m_q\bar{q}q|p\rangle \equiv m_q B_q, \tag{10}$$

$f_{TG}^{(p)} = 1 - \sum_{q=u,d,s} f_{Tq}^{(p)}$ [18], and f_n has a similar expression.

We take the ratios of the quark masses from [19]:

$$\frac{m_u}{m_d} = 0.553 \pm 0.043, \qquad \frac{m_s}{m_d} = 18.9 \pm 0.8, \tag{11}$$

and following [20], we have:

$$z \equiv \frac{B_u - B_s}{B_d - B_s} = 1.49. \tag{12}$$

Defining

$$y \equiv \frac{2B_s}{B_d + B_u}, \tag{13}$$

we then have

$$\frac{B_d}{B_u} = \frac{2 + (z-1)y}{2z - (z-1)y}. \tag{14}$$

The coefficients f_{T_q} are then easily obtained;

$$f_{T_u} = \frac{m_u B_u}{m_p} = \frac{2\Sigma}{m_p(1 + \frac{m_d}{m_u})(1 + \frac{B_d}{B_u})}, \tag{15}$$

$$f_{T_d} = \frac{m_d B_d}{m_p} = \frac{2\Sigma}{m_p(1 + \frac{m_u}{m_d})(1 + \frac{B_u}{B_d})}, \tag{16}$$

$$f_{T_s} = \frac{m_s B_s}{m_p} = \frac{2(\frac{m_s}{m_d})\Sigma y}{m_p(1 + \frac{m_u}{m_d})}. \tag{17}$$

The final task is to determine the quantity y characterizing the density of $\bar{s}s$ in the nucleon.

This may be determined from the π-nucleon Σ term, which is given by

$$\sigma_{\pi N} \equiv \Sigma = \frac{1}{2}(m_u + m_d)(B_u + B_d). \tag{18}$$

We are motivated to reconsider the value of y in light of recent reevaluations of the π-nucleon sigma term Σ, which is related to the strange scalar density in the nucleon by

$$y = 1 - \sigma_0/\Sigma, \tag{19}$$

where σ_0 is the change in the nucleon mass due to the nonzero u, d quark masses, which is estimated on the basis of octet baryon mass differences to be $\sigma_0 = 36 \pm 7$ MeV [21]. In our previous work [4,5], we assumed a relatively conservative value $\Sigma = 45$ MeV, which was already somewhat larger than naive quark model estimates and corresponded to $y \simeq 0.2$. However, recent determinations of the π-nucleon Σ term have found the following values at the Cheng-Dashen point $t = +2m_\pi^2$ [13]:

$$\Sigma_{\rm CD} = (88 \pm 15, 71 \pm 9, 79 \pm 7, 85 \pm 5)\ \text{MeV}. \tag{20}$$

These should be corrected by an amount $-\Delta_R - \Delta_\sigma \simeq -15$ MeV to obtain Σ. Assuming for definiteness the value $\Sigma_{\rm CD} = 79 \pm 7$ MeV, we may estimate

$$\Sigma = (64 \pm 8)\ \text{MeV}. \tag{21}$$

Such a relatively large value of Σ has recently received support from an unexpected quarter, namely, the apparent observation of exotic baryons Θ^+, Ξ^{--} in an antidecuplet of flavor SU(3) [14]. The existence of such states has been a long-standing prediction of chiral-soliton models, but the details of their spectroscopy depend, in particular, on the value of Σ:

$$\frac{m_s}{m}\Sigma = \underbrace{3(4M_\Sigma - 3M_\Lambda - M_N)}_{\text{octet}} + \underbrace{4(M_\Omega - M_\Delta)}_{\text{decuplet}} - \underbrace{4(M_{\Xi^{--}} - M_{\Theta^+})}_{\text{antidecuplet}} \tag{22}$$

in the chiral-soliton model. Inserting the nominal values $M_{\Theta^+} = 1540$ MeV and $M_{\Xi^{--}} = 1862$ MeV, we find $\Sigma = 72$ MeV, corresponding to $y \simeq 0.5$. This determination should be taken with a couple of grains of salt, since it is unclear whether either the Θ^+ or the Ξ^{--} exist. However, since this value is consistent with the more direct estimate (20), we adopt $\Sigma = 64$ MeV and 45 MeV as alternative nominal values, corresponding to $y \simeq 0.45$ and 0.2, respectively, which we use later to discuss the implications of varying Σ.

III. EXPLORATION OF THE CMSSM

We begin by considering the constrained version of the MSSM (CMSSM) [22–24]. This class of models is fully described by four parameters and a sign: a unified gaugino mass $m_{1/2}$, a unified scalar mass m_0, a unified trilinear mass term A_0, and the ratio of the Higgs vacuum expectation values $\tan\beta$. In addition, the sign of the μ parameter also must be specified. The phenomenology of these models has been well studied. The parameters of models with an acceptable cosmological relic density generally fall into one of the following regions: the coannihilation region,[1] where the mass of the neutralino is nearly degenerate with the mass of the stau; the rapid-annihilation funnel, where the mass of the neutralino is close to one-half the mass of the pseudoscalar Higgs boson A; and the focus-point region, which is found at extremely high values of m_0 and is at the edge of the parameter space which allows for radiative electroweak symmetry breaking. We start with an examination of some specific benchmark parameter choices [6,17] that populate these allowed regions.

A. Benchmark scenarios

Figure 1 shows the effect of the value of Σ on the magnitude of the spin-independent elastic χ-proton scattering cross section in the specific cases of the CMSSM benchmark scenarios discussed in [17]. Points A, B, C, D,

[1]Note that, because the relic density has now been determined with high accuracy by cosmological observations [25], and accelerator limits disfavor low $m_{1/2}$, we no longer distinguish a bulk region at low $m_{1/2}$ and m_0 from the coannihilation region.

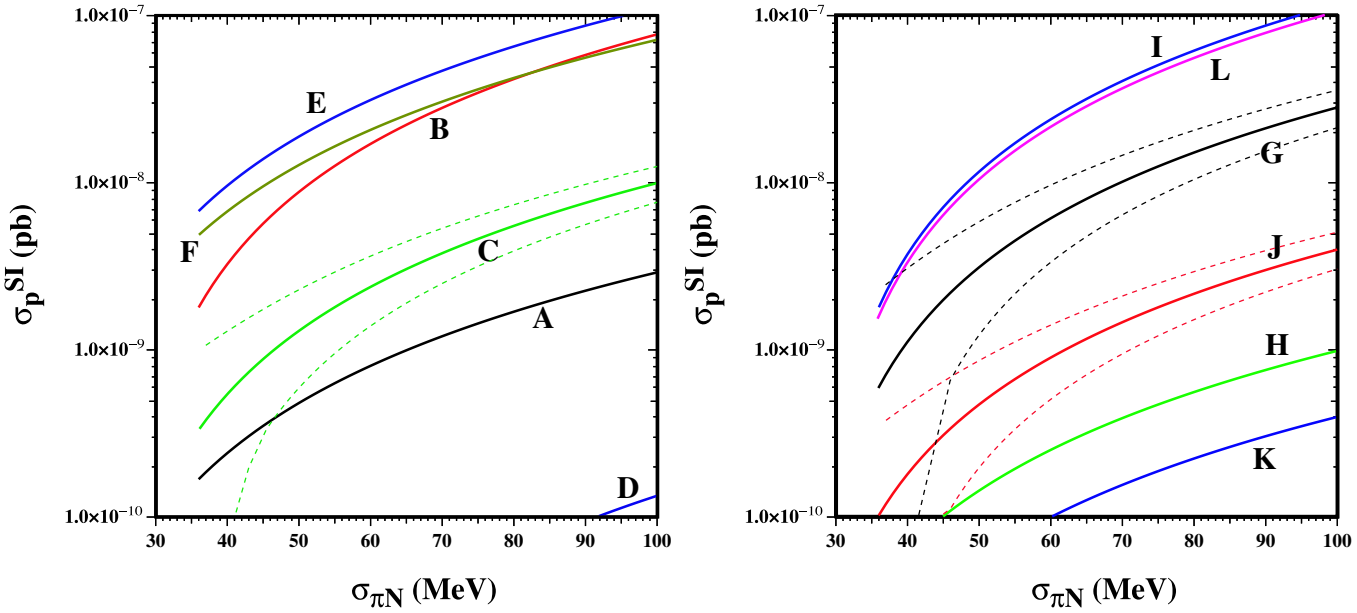

FIG. 1 (color online). The dependences on the π-nucleon Σ term of the elastic cross sections of the benchmark points [17]. The dashed lines indicate the sensitivities to σ_0 in the cases of benchmark scenarios C, G, and J. The predicted cross sections are smaller than the CDMS II upper limits [10] for the models considered, for all Σ values shown.

G, H, I, J, and L are in the coannihilation region; points K and M are in the rapid-annihilation funnels; and points E and F are in the focus-point region. Point M is not shown as its cross section falls below the scale of the plot.[2] It is clear that the value of Σ has quite significant impact in all the scenarios, as indicated by the behaviors of the different lines. There is a general trend for the cross section to increase approximately quadratically with Σ. This would be exact if the $<p|\bar{u}u|p>$ and $<p|\bar{d}d|p>$ contributions were negligible compared with the $<p|\bar{s}s|p>$ contribution. However, Fig. 1 shows that the increasing trend is not exactly universal, reflecting the different relative weights of the various $<p|\bar{q}q|p>$ contributions in the different benchmark scenarios. These depend on $\tan\beta$ and the sign of the Higgs-mixing parameter μ, as can be seen from the formulas in the previous section.

We have plotted in Fig. 1 values of the cross section corresponding to $\Sigma \geq 36$ MeV, i.e., consistent with assuming $y \geq 0$. The dashed curves in Fig. 1 around benchmark points C, G, and J display the effect of the uncertainty in σ_0 as well as the mass ratios which enter into the determination of the f_{T_q} and ultimately the elastic cross section. We see that this uncertainty is not negligible, although that associated with Σ is clearly more important.

We see that, in all scenarios and for all plausible values of Σ, the estimated cross section lies considerably below the current upper limits of CDMS II [10], which can at best exclude models with cross sections larger than 3×10^{-7} pb when $m_\chi = 60$ GeV. If future experiments achieve a sensitivity of 10^{-8} pb, one can plainly see that several of the benchmark scenarios will be probed, particularly if Σ is large.

It is clear from the above discussion that better understanding of the nonperturbative hadronic matrix elements Σ and σ_0 will be needed before the spin-independent elastic-scattering cross section can be predicted accurately in any specific supersymmetric model. This means, in particular, that *unless these hadronic matrix elements can be determined more accurately*, it will be difficult to convert any LHC or LC measurements of MSSM parameters into accurate predictions for elastic-scattering rates, even if they do suffice to calculate accurately the relic LSP density. The experimental determination of Σ is notoriously uncertain: perhaps the time is ripe for another lattice QCD approach?

The benchmark scenarios discussed above were formulated within the CMSSM, and our next step is to explore the CMSSM more generally—to see whether larger cross sections are possible in regions of its parameter space.

B. General analysis of CMSSM models compatible with WMAP

As is well known, for any given value of $\tan\beta$, A_0, and m_t, the CMSSM parameter space consists of narrow strips in the $(m_{1/2}, m_0)$ plane, where the relic density falls within the range allowed for cold dark matter by Wilkinson Microwave Anisotropy Probe (WMAP) and other experi-

[2]These benchmark points were formulated assuming $m_t = 175$ GeV. The small shifts required if one uses the new central value $m_t = 178$ GeV do not impact significantly the cross sections calculated in Fig. 1.

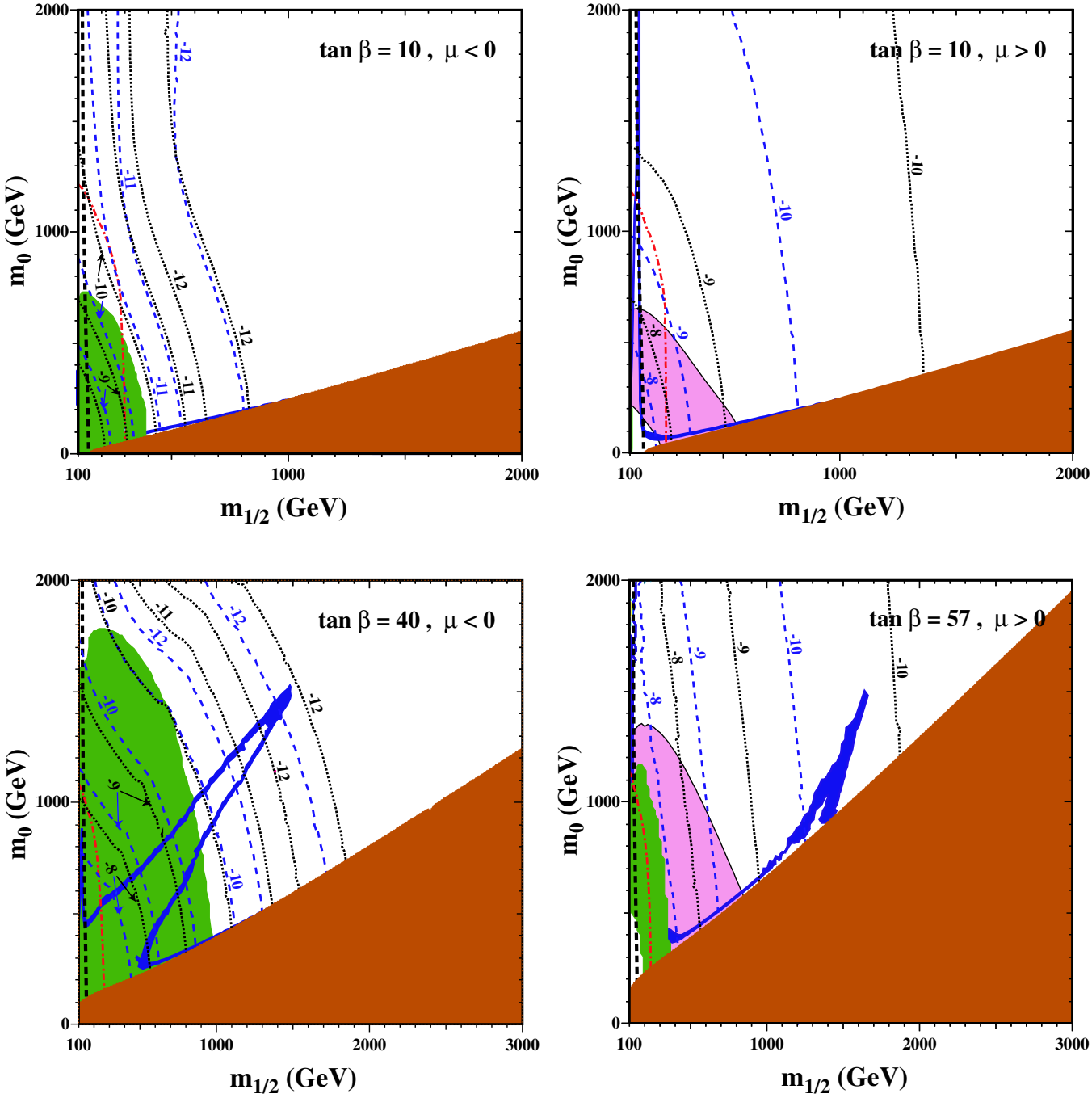

FIG. 2 (color online). The $(m_{1/2}, m_0)$ planes in the CMSSM for (a) $\tan\beta = 10$, $\mu < 0$, (b) $\tan\beta = 10$, $\mu > 0$, (c) $\tan\beta = 40$, $\mu < 0$, and (d) $\tan\beta = 57$, $\mu > 0$, all assuming $A_0 = 0$. We display the WMAP relic-density constraint, the experimental constraints due to m_h, $m_{\chi^\pm}$, $b \to s\gamma$, and $g_\mu - 2$, and contours of the spin-independent elastic-scattering cross section calculated for $\Sigma = 45$ and 64 MeV [lighter (blue) and black dotted contours, respectively), labeled by their exponents in units of picobarns.

ments. In the following, we no longer consider results in the focus-point region: this now appears at very large m_0 if one adopts the new central value $m_t = 178$ GeV,[3] as we do henceforth. At low values of $m_{1/2}$, the length of the strip is in turn restricted by experimental constraints such as m_h, $m_{\chi^\pm}$, and $b \to s\gamma$, whereas at high values of $m_{1/2}$ the strips are truncated by the relic density. We display in Fig. 2 the $(m_{1/2}, m_0)$ planes for $\tan\beta = 10$ and (a) $\mu < 0$; (b) $\mu > 0$; (c) $\tan\beta = 40$, $\mu < 0$; and (d) $\tan\beta = 57$, $\mu > 0$. The latter choices of $\tan\beta$ are close to the maximal values we now find for the corresponding signs of μ. These have increased with the new best-fit value $m_t = 178$ GeV and

[3]We use $m_b(m_b)_{\overline{MS}} = 4.25$ GeV throughout.

recent improvements in our spectrum evaluation code.[4] The rapid-annihilation funnels visible in panels (c, d) are located at values of $m_{1/2}$ that are similar to what we would have found previously for $\tan\beta = 35$, $\mu < 0$ and $\tan\beta = 50$, $\mu > 0$.

Before discussing the effects of the various constraints on the parameter space of the CMSSM, we first comment on the present experimental information concerning $B_s \to \mu^+\mu^-$ decay. The CDF Collaboration has recently published an improved experimental upper limit for this, namely, 5.8×10^{-7} [26]. Since the branching ratio for this decay is proportional to $\tan^6\beta$ at large $\tan\beta$, this constraint potentially could become important. We find that this constraint is currently still contained within the constraints from $b \to s\gamma$, m_h, and $g_\mu - 2$, but this situation may change in the near future.

The various experimental and cosmological constraints on the CMSSM are displayed in various $(m_{1/2}, m_0)$ planes in Fig. 2, but we do not use them all as absolute limits. The dark, tan-shaded regions are, however, completely excluded because there the LSP is charged, being the lighter $\tilde{\tau}$. The thin blue strips are those favored by the WMAP constraint on the relic density of cold dark matter: $0.094 < \Omega_{\rm CDM}h^2 < 0.125$ if $\Omega_\chi \simeq \Omega_{\rm CDM}$, and we also display the restrictions that the accelerator constraints due to m_h [dark (red) dash-dotted lines], $m_{\chi^\pm}$ (black dashed lines) and $b \to s\gamma$ [medium (green) shading] impose on the ranges of $m_{1/2}$ and hence m_0 allowed along the WMAP strips. In general, and specifically for the $b \to s\gamma$ constraint, we exclude the regions of the parameter space that are incompatible with the experiment at the 95% C.L. The constraints that would be imposed by $g_\mu - 2$ at the 2-σ level if the standard model contribution is evaluated using e^+e^- annihilation data alone, neglecting τ decay data, are shown by light (pink) shading in panels (b, d).[5]

Each of the panels also displays contours of the spin-independent elastic-scattering cross section calculated for $\Sigma = 45$ [lighter (blue) dashed contours] and 64 MeV (black dotted contours) labeled by their exponents in units of picobarns. We see that, for $\mu > 0$ in panels (b, d) of Fig. 2, the cross-section contours progress monotonically downward as $m_{1/2}$ increases, with the $\Sigma = 45$ MeV contours always at smaller $m_{1/2}$ than the corresponding contours for $\Sigma = 64$ MeV. However, the progression is not monotonic for $\mu < 0$, as seen in panels (a, c). This is because of the possibility of a cancellation between different contributions to the scattering amplitude [4].

For the purpose of this paper, we choose to treat the WMAP constraint as an upper limit on $\Omega_\chi h^2 \equiv f_\chi \Omega_{\rm CDM} h^2$: $f_\chi \leq 1$, thus allowing for another component of cold dark matter with a fractional density $1 - f_\chi \geq 0$. In this case, the small regions of the $(m_{1/2}, m_0)$ planes between the WMAP strips and the charged LSP corners also are allowed. We can see in Fig. 2 that the spin-independent elastic scattering cross section is very similar in the underdense regions with $f_\chi < 1$, which lie below the WMAP strips and above the charged dark matter region, and also those inside the rapid-annihilation funnels for large $\tan\beta$.

Implementing the accelerator constraints, using the relic density allowed by WMAP as an upper limit: $\Omega_\chi h^2 = f_\chi \Omega_{\rm CDM} h^2$, and rescaling the cross section by a factor f_χ if $f_\chi < 1$, so as to account for the fact that neutralinos could constitute only a fraction f_χ of the galactic halo and that there would be another important local component of cold dark matter, we find the ranges for the effective spin-independent elastic-scattering cross section shown in Fig. 3. These ranges were obtained by statistical sampling of the allowed regions of the CMSSM parameter spaces for the indicated parameter values. The sampling was performed over values of $m_{1/2} = 0.1$ to 2 TeV, $m_0 = 0$ to 2 TeV, $\tan\beta = 2$ to 43 (58) for $\mu < (>)0$, and $A_0 = -3$ to $+3m_{1/2}$. Because of the rescaling and the fact that regions with $f_\chi < 1$ have similar intrinsic cross sections to regions with $f_\chi = 1$, the points with Ω_χ in the range of $\Omega_{\rm CDM}$ favored by WMAP generally appear at the top of the allowed ranges. In general, the calculated cross sections lie below the present CDMS II upper limits, except for certain models with the smallest values of $m_{1/2}$ that are allowed when $\tan\beta \sim 10$ and $\mu > 0$, if one uses $\Sigma = 64$ MeV.

C. Preferred range of sparticle masses

Progressing beyond the above implementation of laboratory experimental constraints, the sparticle mass range preferred within the CMSSM has recently been reassessed [16], in light of recent precision measurements and higher-order calculations in the standard model and the MSSM. As has already been recalled, the anomalous magnetic moment of the muon, $g_\mu - 2$, disagrees with the standard model by between 2.5 and 3 standard deviations [27], if low-energy e^+e^- data are used to estimate the strong-interaction contribution to $g_\mu - 2$: see the light (pink) shaded regions in Fig. 2. The central experimental value favors $\mu > 0$ and $m_{1/2} \sim 300$ GeV for $\tan\beta = 10$,[6] and the preferred value of $m_{1/2}$ increases with $\tan\beta$. The present central values of M_W and $\sin^2\theta_{\rm eff}$ also disagree marginally with the latest theoretical calculations within the standard model. Given the errors, these discrepancies are not significant in themselves, but it so happens that they

[4]The most recent improvements include implementation of the full set of two-loop renormalization group equations.

[5]See [16] for a discussion on the $g_\mu - 2$ deviation range used here. We recall that no models with $\mu < 0$ would be allowed at this significance level.

[6]We note in passing that the minimum of the χ^2 function almost coincides with benchmark point B of [17], to which Point 1a of [28] also is similar.

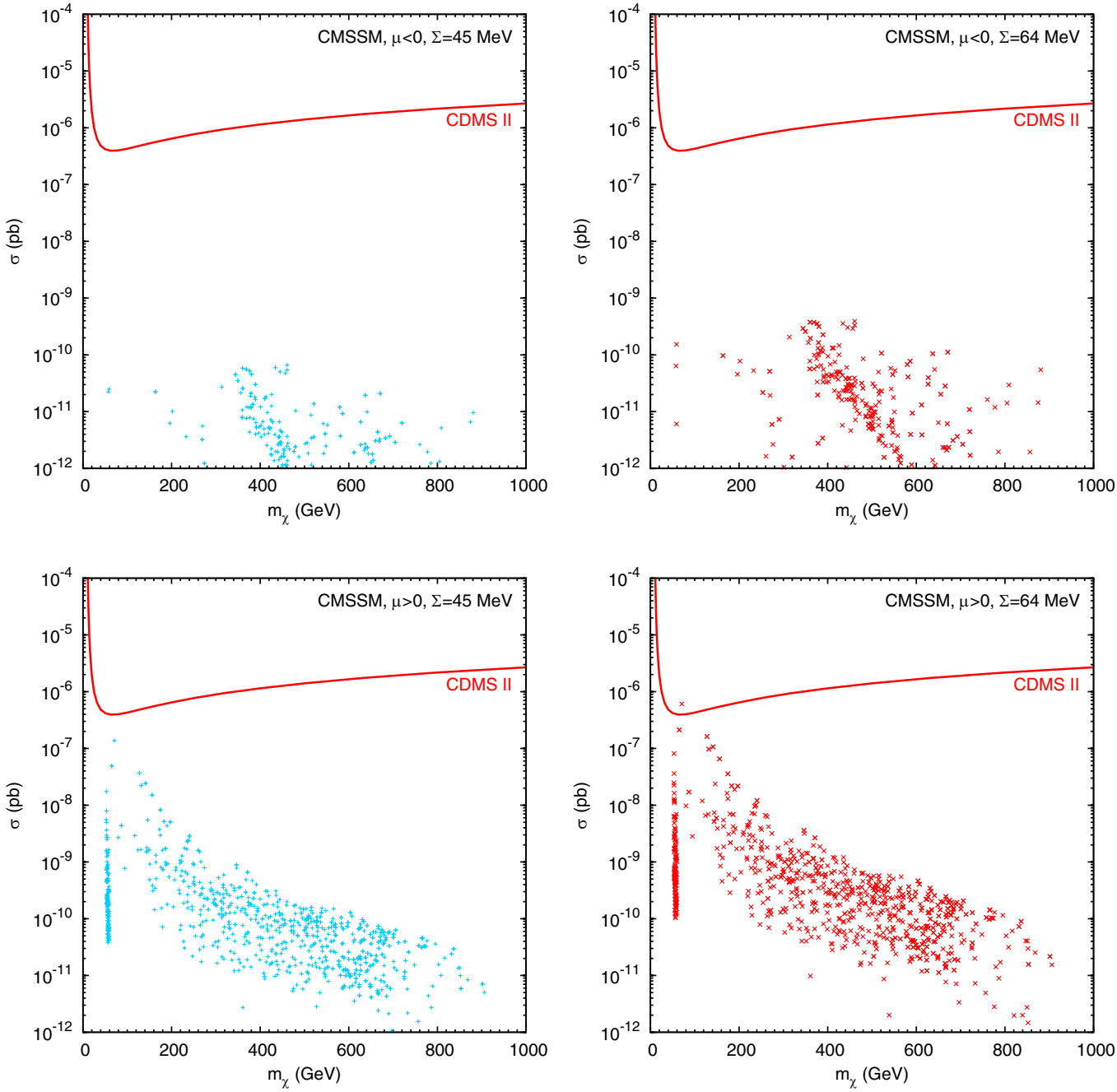

FIG. 3 (color online). Scatter plots of the spin-independent elastic-scattering cross section predicted in the CMSSM for (a, b) $\mu < 0$ and (c, d) $\mu > 0$, with (a, c)$\Sigma = 45$ MeV and (b, d) $\Sigma = 64$ MeV.

are each, separately, best fit also by $m_{1/2} \sim 300$ GeV for $\tan\beta = 10$. The quality of fit in the $(m_{1/2}, A_0)$ planes for $\tan\beta = 10, 50$ has been explored, and the 68% and 90% confidence level regions have been delineated: they stretch up to $m_{1/2} \lesssim 1000$ GeV [16].

In Fig. 4 we display scatter plots of the spin-independent elastic-scattering cross section calculated for $\Sigma = 45$ and 64 MeV, as usual, for the portions of the WMAP strips allowed for (a, b) $\tan\beta = 10$, $\mu > 0$ and (c, d) $\tan\beta = 50$, $\mu > 0$ at both the 68% and 90% confidence levels. The two choices C.L. = 68% and 90 % have different colors [darker (blue) × and lighter (green) + signs, respectively). We do not see large qualitative differences between the cross section predictions in the 68% and 90% confidence level cases. Also, comparing the top and bottom panels, we do not see large qualitative differences between the cross section predictions in the cases $\tan\beta = 10, 50$, though the latter are slightly larger. However, comparing the left and right panels, we once again see the direct effect on the cross section due to our choice of Σ. Since $\mu > 0$ in this analy-

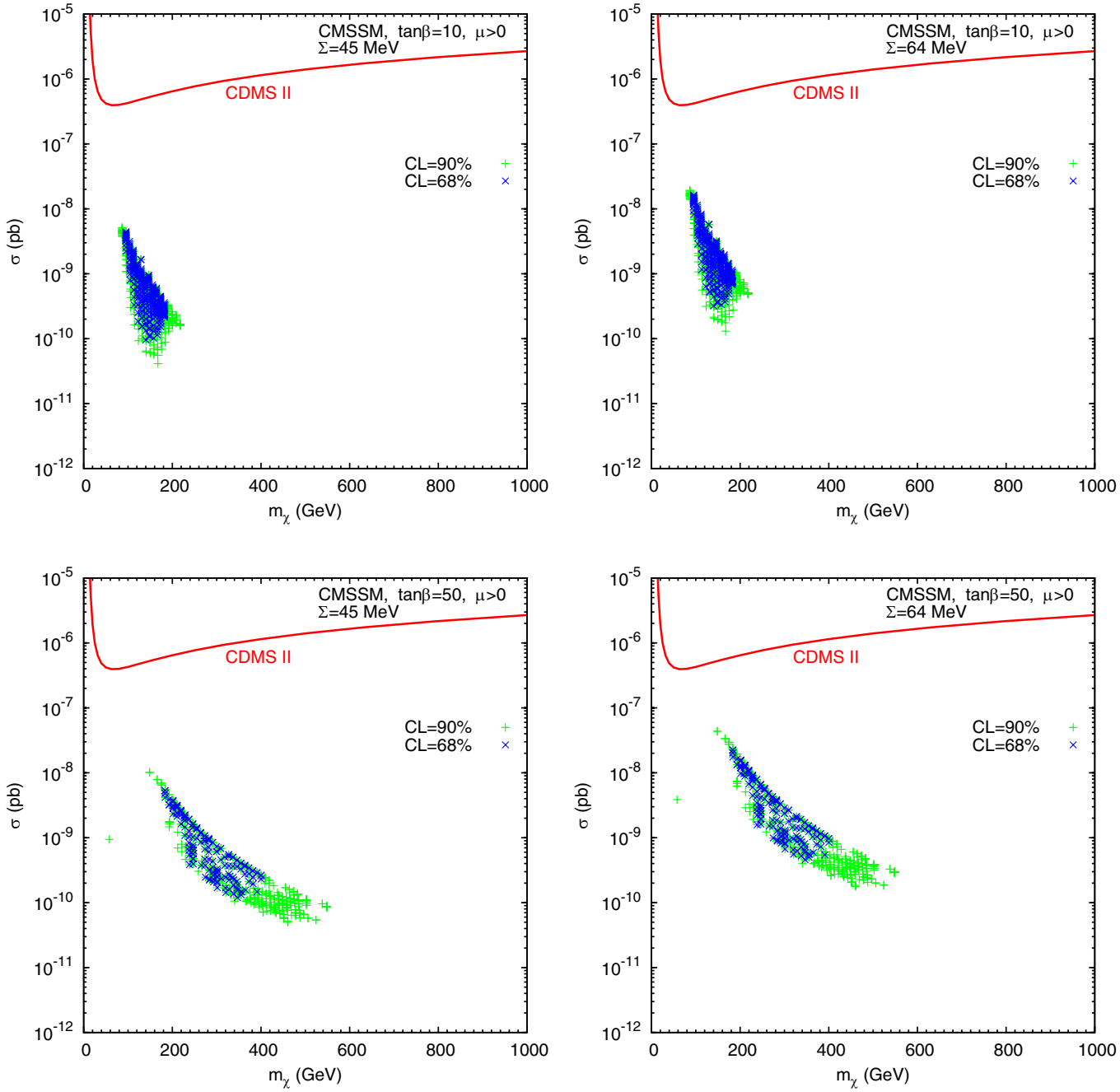

FIG. 4 (color online). Scatter plots of the spin-independent elastic-scattering cross section predicted in the CMSSM for (a, b) $\tan\beta = 10$, $\mu > 0$ and (c, d) $\tan\beta = 50$, $\mu > 0$, with (a, c) $\Sigma = 45$ MeV and (b, d) $\Sigma = 64$ MeV. The predictions for models allowed at the 68% (90%) confidence levels are shown by dark (blue) $\times$ signs [light (green) $+$ signs].

sis, there is no possibility of a cancellation in the cross section. Moreover, comparing with the corresponding panels of Fig. 3, we note that the preferred range of $m_{1/2}$ and hence m_χ happens to be that where the spin-independent elastic scattering cross section is relatively large.

We see that an improvement in the present CDMS II limit by an order of magnitude would just begin to touch the estimated cross section range, for low m_χ and large Σ. On the other hand, an improvement by around 4 orders of magnitude would be required to cover completely all the regions allowed at the 90% confidence level for all the considered range 45 MeV $< \Sigma <$ 64 MeV.

IV. DETECTION IN MODELS WITH NONUNIVERSAL SCALAR MASSES

Larger cross sections may be found in models in which the CMSSM assumptions of universal soft supersymmetry-breaking scalar masses m_0 are relaxed, as we now discuss.

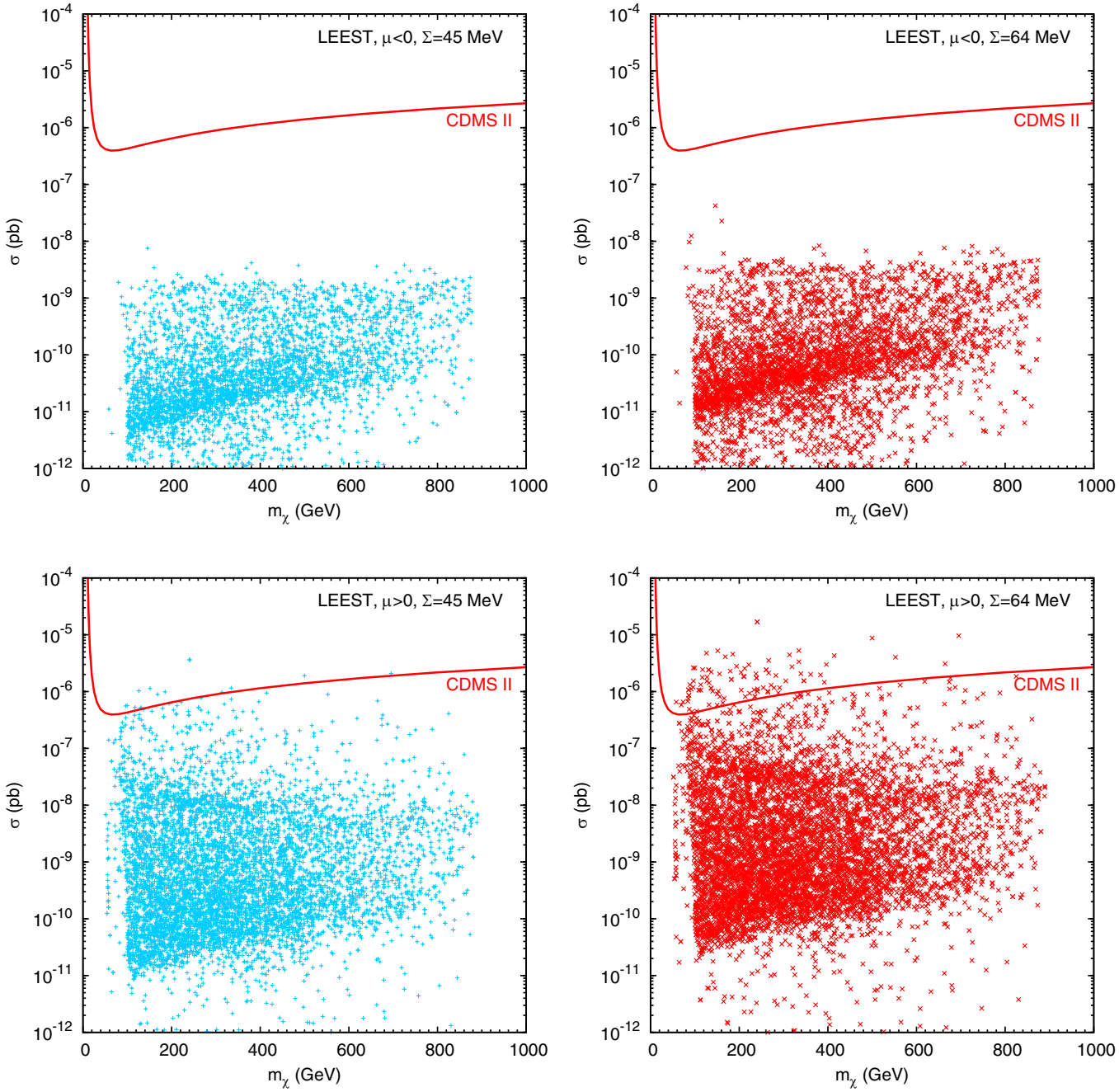

FIG. 5 (color online). As in Fig. 3 but now for the LEEST.

A. General low-energy effective supersymmetric theory

We first consider relaxing the universality assumption for the Higgs bosons and for the soft supersymmetry-breaking squark masses relative to those of the sleptons, requiring only that all the squark and slepton squared masses remain positive under renormalization up to the GUT scale. This we term the most general low-energy effective supersymmetric theory [29]. It is clear that relaxing the CMSSM relationship between the squark and slepton masses $m_{\tilde{q}}, m_{\tilde{\ell}}$ might have a direct impact on the elastic-scattering cross section, although the freedom to adjust $m_{\tilde{q}}/m_{\tilde{\ell}}$ is severely restricted by the LEEST requirement that the squared masses remain positive up to the GUT scale. The primary impact of relaxing universality for the Higgs boson masses is to permit variations from the CMSSM values of the pseudoscalar Higgs mass m_A and the magnitude of Higgs ixing $|\mu|$, which are fixed by the electroweak vacuum conditions. We discuss below the extent to which these different effects can be disentangled.

We display in Fig. 5 scatter plots of the spin-independent elastic-scattering cross section for both signs of the Higgs-mixing parameter μ: negative in panels (a, b) and positive

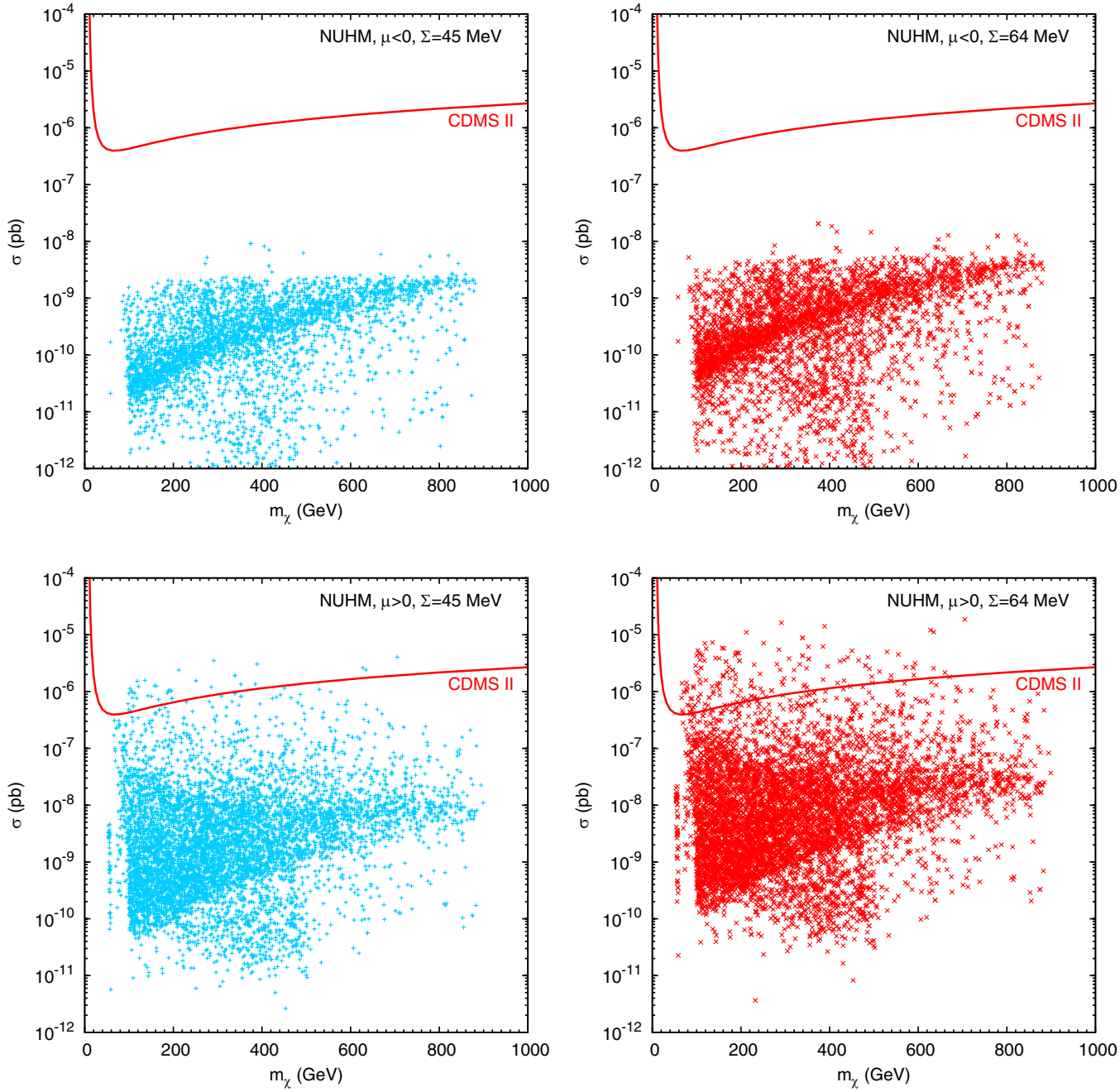

FIG. 6 (color online). As in Fig. 5 but now for the NUHM.

in panels (c, d). Predictions for two values of Σ, the conservative value of 45 MeV, and the more modern value of 64 MeV are shown in panels (a, c) and (b, d), respectively. We see that predictions of Σ for $\mu < 0$ never rise to the sensitivity of the CDMS II experiment [10], whichever value of Σ is used. However, a few points with $m_\chi \lesssim 700$ GeV do exceed the current CDMS II limit for $\mu > 0$, as seen in panels (c, d), particularly when the larger value of Σ is used. We discuss the nature of these excluded points further below.

B. Models with nonuniversal Higgs masses

Since the parameter space of the LEEST has quite a large dimensionality, it is difficult to visualize clearly what classes of models might be excluded by CDMS II. This becomes clearer if one considers a class of models with a lower-dimensional parameter space, namely, those with universal soft supersymmetry-breaking masses for squarks and sleptons but nonuniversal Higgs masses [5,30,31], which allow values of $|\mu|$ and m_A differing from those in

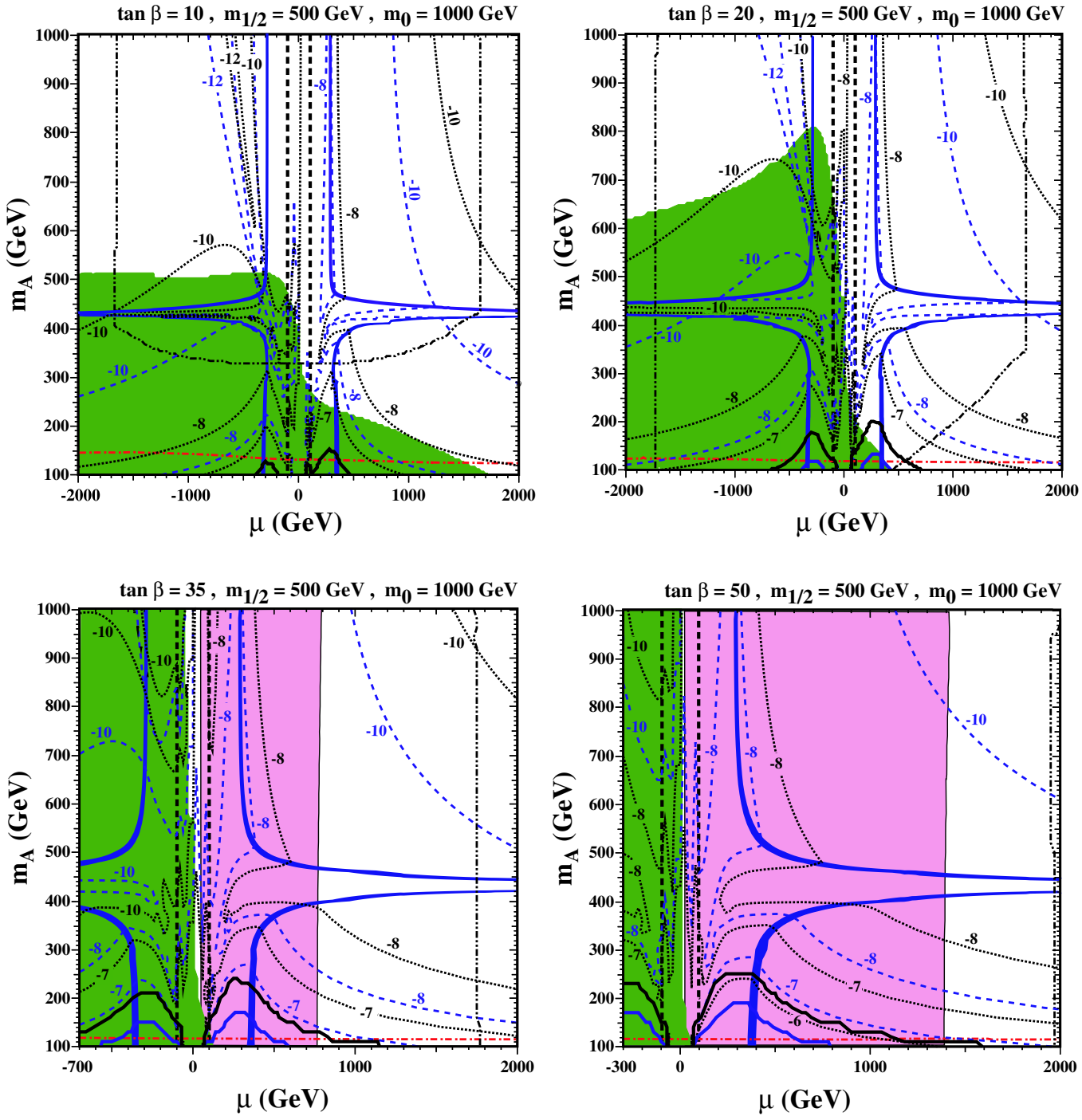

FIG. 7 (color online). Contours of the spin-independent elastic cross section in the (m_A, μ) planes for $(m_{1/2}, m_0) = (500, 1000)$ GeV and $\tan\beta$ = (a) 10, (b) 20, (c) 35, and (d) 50 for $\Sigma = 45$ MeV [dashed (blue) lines] and $\Sigma = 64$ MeV (black dotted lines) labeled by their exponents in units of picobarns. The regions excluded by CDMS II [10] lie below the solid black lines.

the CMSSM. We display in Fig. 6 scatter plots of the spin-independent elastic-scattering cross section for (a, b) $\mu < 0$ and (c, d) $\mu > 0$. The same two choices of Σ, namely, 45 MeV and 64 MeV are made in panels (a, c) and (b, d), respectively.

We see again that no NUHM points can be excluded for $\mu < 0$ but that, as in the LEEST case, some $\mu > 0$ NUHM points may be excluded by CDMS II. This is true, in particular, for the larger choice of Σ. The similarities between the general trends in the corresponding panels of Figs. 5 and 6 suggest that the dominant effects may be due to relaxing the universality assumption for the Higgs masses which, we recall, allows the values of $|\mu|$ and m_A to differ from those in the CMSSM. In fact, the LEEST

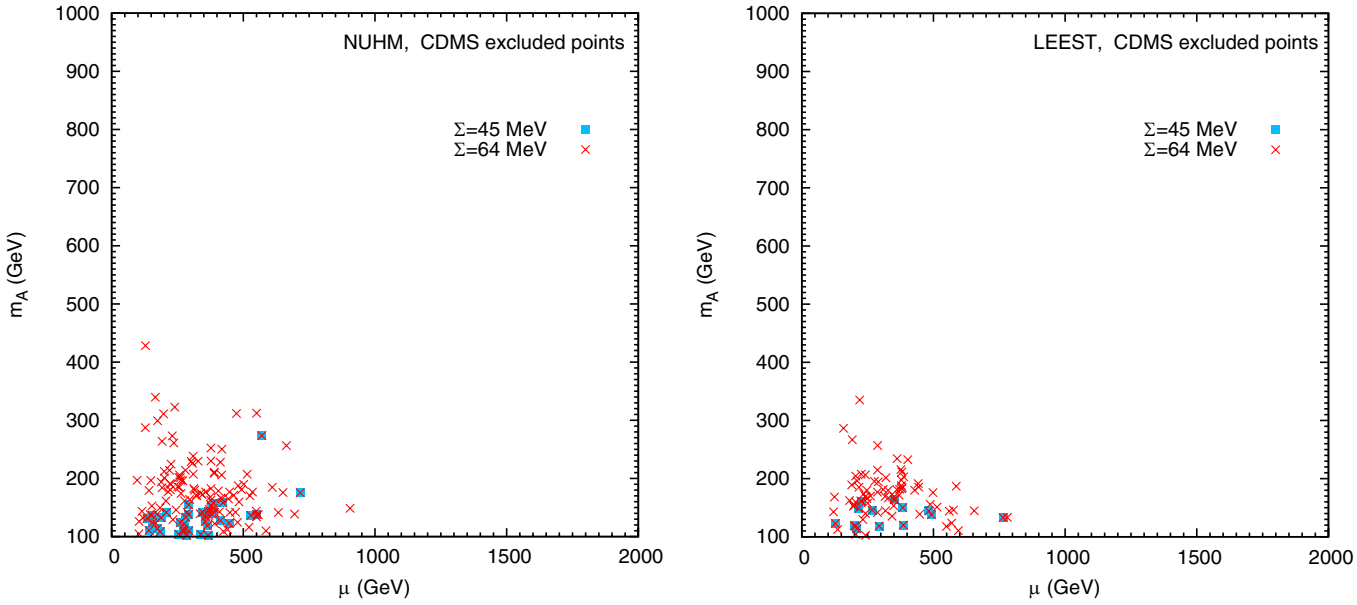

FIG. 8 (color online). Scatter plots in the (μ, m_A) plane of points from (a) Fig. 6(c) and 6(d) and (b) Fig. 5(c) and 5(d) that are excluded by the CDMS II constraint for $\Sigma = 64$ MeV [dark (red) $\times$ signs] or $\Sigma = 45$ MeV [lighter (blue) squares] exhibiting similar clustering at low values of μ and m_A.

does not have much leeway for varying the ratio $m_{\tilde{q}}/m_{\tilde{\ell}}$ at low energies, since we restrict the soft supersymmetry-breaking scalar masses so that the effective scalar squared masses remain nontachyonic all the way up the GUT scale.

The fact that the most significant variations from the CMSSM are likely to be those in $|\mu|$ and m_A is supported by a previous general study of the NUHM [31], in which various $(m_{1/2}, m_0)$, (m_A, μ), and (m_A, M_2) planes were exhibited. The behaviors of the cross section in the NUHM $(m_{1/2}, m_0)$ planes were similar to those found in the CMSSM, varying mainly with $m_{1/2}$ and less with m_0 [5]. The dependence on M_2 in the (m_A, M_2) planes basically reflected the same $m_{1/2}$ dependence. The most striking dependence of the cross section was on $|\mu|$, so we focus here on the (m_A, μ) planes for $m_{1/2} = 500$ GeV, $m_0 = 1000$ GeV and different choices of $\tan\beta$, which are displayed in Fig. 7. Regions outside and below the black double-dash-dotted lines have negative Higgs masses squared below the GUT scale, and are hence unstable, so only the regions between and above these lines are allowed. This constraint becomes less important as $\tan\beta$ is increased.

As usual, the dark (green) shaded regions are excluded by $b \to s\gamma$, the light (pink) shaded regions are those preferred by $g_\mu - 2$, the solid dark (blue) strips are those where Ω_χ falls within the range preferred by WMAP, the medium (red) dash-dotted line is the Higgs mass constraint and the black dashed line is that imposed by the chargino mass. The outward bulges in the WMAP strips are caused by rapid-annihilation funnels. The Higgs constraint forbids regions with low m_A, which are also excluded by the GUT Higgs stability constraint for $\tan\beta = 10$, as seen in Fig. 7(a), but not necessarily for larger values of $\tan\beta$, as seen in the other panels of Fig. 7. The chargino constraint removes regions with small $|\mu|$.

Contours of the spin-independent elastic cross section also are plotted in the (m_A, μ) planes for various values of $\tan\beta$ in Fig. 7, labeled by the exponents in units of picobarns (dashed curves for $\Sigma = 45$ MeV, black dotted curves for $\Sigma = 64$ MeV). We see that the largest values of the spin-independent elastic scattering cross section occur when μ and m_A are relatively small. Also displayed in Fig. 7 are the regions excluded by the CDMS II upper limit (solid black line), including also the factor $f_\chi < 1$ where appropriate for models with $\Omega_\chi < \Omega_{\rm CDM}$. In panel (a) for $\tan\beta = 10$, the regions excluded by CDMS II were already excluded by the GUT Higgs stability and $b \to s\gamma$ constraints. However, in the other panels we see that there are regions at low μ and m_A that were allowed by the other constraints but are now excluded by CDMS II. These regions become progressively more extensive as $\tan\beta$ increases.

These regions are reflected in Fig. 8(a), which displays in the (μ, m_A) plane the NUHM points from Fig. 6(c) and 6(d) that are excluded by the CDMS II result if one assumes $\Sigma = 64$ MeV [dark (red) $\times$ signs] or $\Sigma = 45$ MeV [lighter (blue) squares]. As expected, they cluster at small values of μ and m_A.[7] Their values of μ and m_A are

[7]Analogous high-cross-section points for $\mu < 0$ are excluded by the $b \to s\gamma$ constraint, as seen in Fig. 7.

generally smaller than those of the benchmark points [17], which are all compatible with CDMS II, as we saw in Fig. 1. For comparison, only benchmark point B ($m_A \sim 370$ GeV) has a pseudoscalar mass less than 400 GeV and all but points B, I ($m_A \sim 450$ GeV), and L ($m_A \sim 490$ GeV) have pseudoscalar masses in excess of 500 GeV. Similarly, with the exception of the focus points (E and F), typical values μ are relatively large. Point B has $\mu \sim 330$ GeV, point I has $\mu \simeq 440$ GeV, and G has $\mu \simeq 470$ GeV, whereas all other points have μ in excess of 500 GeV. Figure 8(b) is the corresponding plot for the excluded LEEST points from Fig. 5(c) and 5(d). This exhibits very similar features, confirming the importance of these variables also in the LEEST scenario. In contrast, the ratios $m_{\tilde{q}}/m_{\tilde{\ell}}$ for the excluded LEEST points do not exhibit any clustering at low values.

V. CONCLUSIONS AND PROSPECTS

In this paper, we have made a new comparison between theoretical predictions of the spin-independent cross section for the elastic scattering of supersymmetric dark matter and the improved experimental upper limit recently provided by CDMS II [10]. In making this comparison, we have contrasted the theoretical predictions made with different estimates of the π-nucleon Σ term. Larger values may be supported by recent reports of exotic baryons, but these do not increase greatly the ranges of theoretical models excluded by CDMS II. We also have incorporated in our analysis the new central value of m_t, which enters indirectly into constraints on the supersymmetric parameter space and into relic-density calculations.

Some supersymmetric models with nonuniversal Higgs masses are now excluded by the CDMS II upper limit, as are some models which also incorporate nonuniversal squark and slepton masses. These are mainly models with the smaller values of $|\mu|$ and/or m_A that become allowed when the universality conditions are relaxed for the Higgs masses.

On the other hand, only very small parts of the CMSSM parameter space are yet excluded. Specifically, the cross sections we find in the supersymmetric benchmark scenarios of [17] all lie considerably below the CDMS II sensitivity, as do all points allowed at the 68% or even 90% confidence level by a recent likelihood [16] analysis of the CMSSM parameter space incorporating information on m_W, $\sin^2\theta_{\rm eff}$ and $g_\mu - 2$.

An improvement over the present CDMS II sensitivity by about an order of magnitude would begin to challenge the preferred region of CMSSM parameter space, but an improvement by about 4 orders of magnitude would be required to cover it completely. We conclude that direct searches for supersymmetric dark matter are just beginning to reach interesting sensitivities, but that considerable improvement will be needed to exclude (or hopefully discover) supersymmetric dark matter.

ACKNOWLEDGMENTS

The work of K. A. O. and V. C. S. was supported in part by DOE Grant No. DE-FG02-94ER-40823. We would like to thank Rick Gaitskell for information regarding CDMS II data. Y. S. would like to thank M. Voloshin for helpful discussions and the Perimeter Institute for its hospitality.

[1] J. Ellis, J. S. Hagelin, D. V. Nanopoulos, K. A. Olive, and M. Srednicki, Nucl. Phys. **B238**, 453 (1984); see also H. Goldberg, Phys. Rev. Lett. **50**, 1419 (1983).

[2] K. Griest, Phys. Rev. D **38**, 2357 (1988); J. Ellis and R. Flores, Nucl. Phys. **B307**, 883 (1988); R. Barbieri, M. Frigeni, and G. Giudice, Nucl. Phys. **B313**, 725 (1989); R. Flores, K. A. Olive, and M. Srednicki, Phys. Lett. B **237**, 72 (1990); J. Ellis and R. Flores, Phys. Lett. B **263**, 259 (1991); J. Ellis and R. Flores, Phys. Lett. B **300**, 175 (1993); M. Drees and M. M. Nojiri, Phys. Rev. D **48**, 3483 (1993); V. Bednyakov, H. V. Klapdor-Kleingrothaus, and S. Kovalenko, Phys. Rev. D **50**, 7128 (1994); R. Arnowitt and P. Nath, Phys. Rev. D **54**, 2374 (1996); L. Bergstrom and P. Gondolo, Astropart. Phys. **5**, 263 (1996); H. Baer and M. Brhlik, Phys. Rev. D **57**, 567 (1998); A. Corsetti and P. Nath, Phys. Rev. D **64**, 125010 (2001).

[3] E. Accomando, R. Arnowitt, B. Dutta, and Y. Santoso, Nucl. Phys. **B585**, 124 (2000); R. Arnowitt, B. Dutta, and Y. Santoso, hep-ph/0005154.

[4] J. Ellis, A. Ferstl, and K. A. Olive, Phys. Lett. B **481**, 304 (2000); J. Ellis, A. Ferstl, and K. A. Olive, Phys. Rev. D **63**, 065016 (2001); J. R. Ellis, A. Ferstl, and K. A. Olive, Phys. Lett. B **532**, 318 (2002).

[5] J. R. Ellis, A. Ferstl, K. A. Olive, and Y. Santoso, Phys. Rev. D **67**, 123502 (2003).

[6] J. R. Ellis, J. L. Feng, A. Ferstl, K. T. Matchev, and K. A. Olive, Eur. Phys. J. C **24**, 311 (2002).

[7] For other scattering calculations, see, for example, J. L. Feng, K. T. Matchev, and F. Wilczek, Phys. Lett. B **482**, 388 (2000); M. Drees, Y. G. Kim, T. Kobayashi, and M. M. Nojiri, Phys. Rev. D **63**, 115009 (2001); Y. G. Kim and M. M. Nojiri, Prog. Theor. Phys. **106**, 561 (2001); A. B. Lahanas, D. V. Nanopoulos, and V. C. Spanos, Mod. Phys. Lett. A **16**, 1229 (2001); A. B. Lahanas, D. V. Nanopoulos, and V. C. Spanos, Phys. Lett. B **518**, 94 (2001); E. A. Baltz and P. Gondolo, Phys. Rev. Lett. **86**, 5004 (2001); Y. G. Kim, T. Nihei, L. Roszkowski, and R. Ruiz de Austri, J. High Energy Phys. 12 (2002) 034; M. E. Gómez and J. D. Vergados, Phys. Lett. B **512**, 252 (2001); H. Baer, C. Balazs, A. Belyaev, and J. O'Farrill, J. Cosmol. Astropart.

Phys. 09 (2003) 007.

[8] A. Bottino, F. Donato, N. Fornengo, and S. Scopel, Phys. Rev. D **59**, 095003 (1999); Phys. Rev. D **59**, 095004 (1999); Phys. Rev. D **63**, 125003 (2001); R. Arnowitt and P. Nath, Phys. Rev. D **60**, 044002 (1999); R. Arnowitt, B. Dutta, and Y. Santoso, Nucl. Phys. **B606**, 59 (2001).

[9] A. Bottino, F. Donato, N. Fornengo, and S. Scopel, Astropart. Phys. **13**, 215 (2000); Astropart. Phys. **18**, 205 (2002).

[10] D. S. Akerib *et al.* (CDMS Collaboration), Phys. Rev. Lett. **93**, 211 301 (2004).

[11] D. Abrams *et al.* (CDMS Collaboration), Phys. Rev. D **66**, 122003 (2002); A. Benoit *et al.*, Phys. Lett. B **545**, 43 (2002).

[12] R. Bernabei *et al.* (DAMA Collaboration), Phys. Lett. B **480**, 23 (2000).

[13] M. M. Pavan, I. I. Strakovsky, R. L. Workman, and R. A. Arndt, PiN Newslett. **16**, 110 (2002).

[14] P. Schweitzer, Eur. Phys. J. A **22**, 89 (2004); J. R. Ellis, M. Karliner, and M. Praszalowicz, J. High Energy Phys. 05 (2004) 002.

[15] CDF Collaboration, D0 Collaboration, and Tevatron Electroweak Working Group, hep-ex/0404010.

[16] J. R. Ellis, S. Heinemeyer, K. A. Olive, and G. Weiglein, J. High Energy Phys. 02 (2005) 013.

[17] M. Battaglia *et al.*, Eur. Phys. J. C **22**, 535 (2001); M. Battaglia, A. De Roeck, J. R. Ellis, F. Gianotti, K. A. Olive, and L. Pape, Eur. Phys. J. C **33**, 273 (2004).

[18] M. A. Shifman, A. I. Vainshtein, and V. I. Zakharov, Phys. Lett. **78B**, 443 (1978); A. I. Vainshtein, V. I. Zakharov, and M. A. Shifman, Usp. Fiz. Nauk **130**, 537 (1980).

[19] H. Leutwyler, hep-ph/9609465.

[20] H.-Y. Cheng, Phys. Lett. B **219**, 347 (1989).

[21] J. Gasser, H. Leutwyler, and M. E. Sainio, Phys. Lett. B **253**, 252 (1991); M. Knecht, PiN Newslett. **15**, 108 (1999); M. E. Sainio, PiN Newslett. **16**, 138 (2002).

[22] J. R. Ellis, T. Falk, G. Ganis, K. A. Olive, and M. Srednicki, Phys. Lett. B **510**, 236 (2001); V. D. Barger and C. Kao, Phys. Lett. B **518**, 117 (2001); L. Roszkowski, R. Ruiz de Austri, and T. Nihei, J. High Energy Phys. 08 (2001) 024; A. B. Lahanas and V. C. Spanos, Eur. Phys. J. C **23**, 185 (2002); A. Djouadi, M. Drees, and J. L. Kneur, J. High Energy Phys. 08 (2001) 055; U. Chattopadhyay, A. Corsetti, and P. Nath, Phys. Rev. D **66**, 035003 (2002); H. Baer, C. Balazs, A. Belyaev, J. K. Mizukoshi, X. Tata, and Y. Wang, J. High Energy Phys. 07 (2002) 050; R. Arnowitt and B. Dutta, hep-ph/0211417; J. R. Ellis, K. A. Olive, Y. Santoso, and V. C. Spanos, Phys. Lett. B **573**, 162 (2003).

[23] J. R. Ellis, K. A. Olive, Y. Santoso, and V. C. Spanos, Phys. Lett. B **565**, 176 (2003).

[24] H. Baer and C. Balazs, J. Cosmol. Astropart. Phys. 05 (2003) 006; A. B. Lahanas and D. V. Nanopoulos, Phys. Lett. B **568**, 55 (2003); U. Chattopadhyay, A. Corsetti, and P. Nath, Phys. Rev. D **68**, 035005 (2003); C. Munoz, Int. J. Mod. Phys. A **19**, 3093 (2004); R. Arnowitt, B. Dutta, and B. Hu, hep-ph/0310103.

[25] C. L. Bennett *et al.*, Astrophys. J. Suppl. Ser. **148**, 1 (2003); see also D. J. Eisenstein *et al.* (Sloan Digital Sky Syurvey Collaboration), astro-ph/0501171.

[26] D. Acosta *et al.* (CDF Collaboration), Phys. Rev. Lett. **93**, 032 001 (2004).

[27] G. W. Bennett *et al.* (Muon g-2 Collaboration), Phys. Rev. Lett. **92**, 161 802 (2004).

[28] B. C. Allanach *et al.*, in *Proceedings of the APS/DPF/DPB Summer Study on the Future of Particle Physics (Snowmass 2001)*, edited by N. Graf [Eur. Phys. J. C 25, 113 (2002), eConf, C010630, P125 (2001)].

[29] J. R. Ellis, K. A. Olive, Y. Santoso, and V. C. Spanos, Phys. Lett. B **573**, 162 (2003).

[30] M. Drees, M. M. Nojiri, D. P. Roy, and Y. Yamada, Phys. Rev. D **56**, 276 (1997); **64**, 039901(E) (1997); M. Drees, Y. G. Kim, M. M. Nojiri, D. Toya, K. Hasuko, and T. Kobayashi, Phys. Rev. D **63**, 035008 (2001); V. Berezinsky, A. Bottino, J. R. Ellis, N. Fornengo, G. Mignola, and S. Scopel, Astropart. Phys. **5**, 1 (1996); P. Nath and R. Arnowitt, Phys. Rev. D **56**, 2820 (1997); A. Bottino, F. Donato, N. Fornengo, and S. Scopel, Phys. Rev. D **63**, 125003 (2001); S. Profumo, Phys. Rev. D **68**, 015006 (2003).

[31] J. Ellis, K. Olive, and Y. Santoso, Phys. Lett. B **539**, 107 (2002); J. R. Ellis, T. Falk, K. A. Olive, and Y. Santoso, Nucl. Phys. **B652**, 259 (2003).